ROYAL SOCIETY
OF CHEMISTRY

PAPER

Check for updates

Topological defects stabilized by a soft twist-bend dimer and quantum dots lead to a wide thermal range and ultra-fast electro-optic response in a liquid crystalline amorphous blue phase†

Nurjahan Khatun, [ID] [ab] Vimala Sridurai,[a] Katalin F. Csorba[c] and Geetha G. Nair [ID] *[a]

Amorphous Blue phase, or BPIII, a mesophase exhibited by highly chiral liquid crystals, is increasingly being investigated for next-generation displays due to its attractive electro-optical properties, such as sub-millisecond response time, high contrast ratio and wide viewing angle. However, obtaining a fast-responding, thermally stable BPIII with commercial usability is still a challenge due to the frustrated nature of the phase. The study presented here investigates the thermal and electro-optic properties of the BPIII exhibited by a low molecular weight liquid crystalline system. Adding a twist-bend nematic dimer to a mixture comprising a nematic liquid crystal and chiral dopant helps stabilize the BPI, the cubic blue phase, due to the ultra-low bend elastic constant and saddle-splay deformation inherent to the dimer. Doping small concentrations of surface-functionalized quantum dots reduces the free energy associated with the topological defects leading to a complete transformation of the cubic blue phase to an amorphous one, with the latter exhibiting a wide thermal range. Polarizing optical microscopy, and electro-optical studies confirm the existence of BPIII over 34 °C spanning ambient and below/above ambient temperatures. The response time associated with the switching between achromatic dark and bright states is ~200 μs, a value faster than that reported for low molecular weight systems and on par with polymeric ones. Furthermore, the BPIII exhibits a hysteresis-free optical transmittance with low operating voltages and high contrast ratio. A prototype device fabricated using the BPIII composite is found to be thermally, temporally and electrically stable, making it highly promising for display device applications.

1. Introduction

Liquid crystal display (LCD) technology based on conventional nematic liquid crystals has seen tremendous growth in recent decades, finding wide applications in televisions, computers, and mobile phone screens. The improvements, such as LED-backlighting and IPS switching, have greatly enhanced the capabilities of LCD in terms of vibrant colour gamut, wider viewing angle, image brightness, energy efficiency, cost-effectiveness, the durability of the pixels, and robustness against burnout (image persistence).[1–5] Yet, LCD suffers in terms of response time and

[a] *Centre for Nano and Soft Matter Sciences, Bangalore 562162, India. E-mail: geeraj88@gmail.com*
[b] *Manipal Academy of Higher Education, Manipal 576104, India*
[c] *Research Institute for Solid State Physics and Optics of the Hungarian Academy of Sciences Budapest, Hungary*

† Electronic supplementary information (ESI) available: Chemical structures and compositions of the materials, optical microscopy, phase sequence of the composites, HRTEM, UV-Vis and PL spectra of the QDs, circular dichroism, DSC, electro-optical switching and switching video. See DOI: https://doi.org/10.1039/d3tc00861d

hence, is not on par with the recently developed OLED display technology.[5] The active material used in LCDs is the rod-shaped nematic liquid crystal, which has a switching speed of a few tens of milliseconds,[1,5] much slower compared to the sub-millisecond response of OLEDs. Therefore, finding an alternative material that is stable over a wide thermal range, including ambient temperatures and exhibiting a sub-millisecond response is essential to unlocking the full potential of LCD technology. In this context, blue phase III (BPIII), a unique mesophase exhibited by highly chiral liquid crystal (LC) materials, is being explored as a potential candidate for next-generation LCDs.

Blue phase (BP), an optically isotropic LC phase, typically appears between the cholesteric or chiral nematic (Ch) and isotropic (Iso) phases in the thermal scale.[6–8] Due to the high chirality, the LC molecules self-assemble to form double twisted cylinders (DTCs), and disclination lines appear when the DTCs meet each other. Based on the arrangement of DTCs, BP is classified into three subphases, namely BPI, BPII, and BPIII.[6] In BPI and BPII, DTCs organize periodically to form body-centred cubic and simple cubic structures, respectively. The lattice constant of the cubic structures is of the order of

several hundred nanometers,[7–9] and therefore BPI and BPII selectively reflect colors along all three directions in the visible spectrum, a characteristic of 3D photonic crystals.[7,10–14] The cubic BPs have potential applications[15–20] in reflecting displays, optical filters, and lasers. The BPIII, also known as "blue fog", has the DTCs arranged randomly, and hence an amorphous structure.[21,22] Being optically isotropic, the BPIII appears dark when viewed between a pair of crossed polarizers. On application of an in-plane electric field, the DTCs unwind, and the LC molecules orient along the field direction giving rise to a bright state.

In terms of display device parameters, BPIII is known to have several advantages over the conventional nematic phase.[23–27] For example, BPIII does not require an alignment layer, unlike nematic, making the device fabrication simple and cost-effective. The response time of BPIII is in the sub-millisecond regime, on par with that of OLEDs. The switching between the achromatic dark (at zero fields) and the bright (on application of electric field) states gives rise to a high contrast ratio. Furthermore, the BPIII is known to exhibit a wide and symmetric viewing angle as well.

However, BPIII suffers from certain drawbacks such as low thermal stability, high operating voltages, and hysteresis due to residual transmittance,[28] impeding its commercial usage in display devices. Kikuchi et al. achieved BPI with a wide thermal range of 60 °C by polymer stabilization, the first successful method to stabilize a BP.[29] A similar technique is also implemented for BPIII by Kim et al. and further improved by Gandhi et al. via polymer templating.[30,31] Although such systems exhibit sub-millisecond switching time, the operating voltages remain relatively high due to the presence of a strong polymer network.

Several attempts have been made to thermally stabilize the BPIII in low molecular weight systems with improved display parameters. Some of the techniques used are nanoparticle inclusion,[32–34] and addition of bent-core[35–37] and T-shaped[38–41] materials. Although the addition of nanoparticles such as quantum dots (QDs)[32–34] and bent-core materials[35,36] is known to stabilize BPIII, electro-optic studies are not reported in several of the systems. Yoshizawa and co-workers have extensively studied the usage of T-shaped mesogens to stabilize BPIII over a thermal range of ∼33 °C, yet, the phase is stable only at sub-ambient temperatures.[41] Also, the response time reported for the system is in the range of hundreds of milliseconds.[41] The BPIII systems reported by Chen et al. exhibit response times in the range of a few milliseconds, but the thermal stability is ∼10 to 15 °C, close to only ambient temperatures.[42,43] Hence, obtaining a BPIII system stable over a wide thermal range, spanning above ambient, ambient and sub-ambient temperatures along with sub-millisecond response time and low operating voltages is extremely important from the viewpoint of display applications.

The current study is an attempt to achieve a thermally stable high-performing BPIII by the addition of a twist-bend nematic dimeric compound (NTB) and surface-functionalized QDs to a low molecular weight liquid crystalline system consisting of a chiral dopant (CD) and a nematic liquid crystal (NLC). The optimized QD-doped BPLC system shows a wide thermal range of BPIII (∼34 °C) covering ambient, above- and sub-ambient temperatures along with hysteresis-free sub-millisecond response times, low operating voltages and high contrast ratio.

2. Experimental section

2.1. Materials

The nematic LC (NLC) used is BL036 (Merck, UK), a eutectic mixture of seven components, exhibiting positive dielectric anisotropy. A left-handed chiral material, S811 (Merck, Japan), is used as the chiral dopant (CD) to induce BP. A compound exhibiting the twist-bend nematic phase, 1″,7″-bis(4-cyanobiphenyl-4′-yl)heptane, NTB for short (Synthon Chemicals, Germany), is added to thermally stabilize the cubic BP. A bent-core LC, 4,6-dichloro-1,3-phenylene bis[4′-(10-undecenyloxy)]-1,1′-biphenyl-4-carboxylate, BLC for short, synthesized in our laboratory is used to prepare a BPLC mixture for the control experiment. The core-shell type quantum dots, CdSe (core)/ZnS (shell) (QD for short) tethered with the ligand octadecylamine (ODA) (Sigma Aldrich), are used as nanoparticle inclusions to the host BPLC. The structure and composition of the materials used are shown in Fig. S1, Section S1, ESI.†

2.2. Sample preparation

The BPLC composites are prepared by carefully weighing the individual components, NLC, CD and NTB/BLC, using an ultra-microbalance (Sartorious, SE2) and mixing them thoroughly at 120 °C, a temperature much higher than the isotropic temperature of any of the components. The homogeneity of the composites is confirmed by examining the phase transition temperatures using polarizing optical microscopy (details given below). The host BPLC is optimized for the thermal stability of BP in two steps: (i) the concentration of CD in NLC is varied by fixing the concentration of NTB and (ii) the NTB concentration is varied while keeping the concentration of CD constant. The concentration of the surface-functionalized QD in the host BPLC is kept very small, i.e., 0.005 wt%, to obtain the QD-doped BPLC composite (QD-BPLC for short). Prior to the addition to the host BPLC, the stock solution of CdSe/ZnS (the QD) in toluene is sonicated for about 30 minutes to eliminate any possible aggregation of the particles. Then a pre-determined volume of the QD solution along with excess toluene (solvent) is added to the host BPLC, and the mixture is stirred continuously for three days at 100 °C to evaporate the solvent and achieve a homogeneous dispersion of QD in the host BPLC. The remaining traces of solvent are evaporated by vacuum drying.

2.3. Characterization of QDs

2.3.1. High-resolution transmission electron microscopy (HRTEM). HRTEM studies of QDs are carried out using the JEOL JEM 2100 field emission transmission electron microscope at an accelerating voltage of 200 kV with the sample mounted on a copper grid. From the HRTEM images, the size of the QDs is determined to be ∼5.8 ± 0.7 nm by analyzing 100 particles using ImageJ software. The high-resolution images clearly show the presence of lattice fringes, and the selected area electron diffraction (SAED) shows bright spots, indicating

that the QDs are crystalline in nature. The HRTEM images and SAED patterns are shown in Fig. S2, Section S2, ESI.†

2.3.2. Absorption and emission spectroscopy. The absorption and emission spectra are obtained using a UV–Vis-NIR spectrophotometer (Perkin Elmer, Lambda750) and Photoluminescence spectrophotometer (Horiba Jobin Yvon, Flurolog-3), respectively. The spectra, as shown in Fig. S3 (Section S2, ESI†), indicate a strong absorption at 563 nm and a corresponding emission at 580 nm.

2.4. Polarizing optical microscopy (POM)

A polarizing optical microscope (*Leica* – DM4500P) in conjunction with a temperature-controlled hot stage (*Mettler Toledo* – HS82/HS1) is used to identify the mesophases and phase transition temperatures. The composites are filled in indium tin oxide (ITO) coated test cells with a cell gap of ~10 μm and/or in-plane switching cells (discussed below) in the isotropic phase by capillary action. The textural images are captured *in situ* using a CCD camera (*Lumenera* – *Infinity*3) fixed to the POM.

2.5. Circular dichroism

The circular dichroism studies are carried out using a Circular Dichroism Spectropolarimeter (*Jasco J* – 810) in conjunction with a temperature-controlled hot stage (*Mettler Toledo* – HS82/HS1) to detect the chirality of the mesophase.

2.6. Differential scanning calorimetry (DSC)

DSC experiments are carried out using DSC (*PerkinElmer* 8000) both on heating and cooling cycles at the rate of 5 °C min^{-1} to determine the phase transition temperatures.

2.7. Electro-optical studies

The composite QD-BPLC is filled in an in-plane switching (IPS) test cell (from INSTEC Inc, USA) with inter-digitated ITO electrodes patterned on one of the glass substrates to determine the threshold voltage and the response times. The width of the electrodes and the gap between the interdigitated electrodes are identical, *i.e.*, 10 μm, and the gap between the top and bottom substrates, which defines the cell thickness, is 7.5 μm. The test cell filled with the sample is placed inside the hot stage such that the long axis of the inter-digitated electrodes is at 45° with respect to the polarization axis of either the polarizer or the analyzer. An ac electric field (sine, 10 kHz) is applied to the sample using a waveform generator (*Agilent* – 3320A) in conjunction with a high voltage amplifier (*Trek* – PZD700A). The light from the microscope lamp is incident on the sample, and the transmitted light intensity through the sample is collected using a photodiode (*Hamamatsu* – S2281) with a wideband amplifier (*Hamamatsu* – C9329). The output of the photodiode is fed to a digital multimeter (*Keithley* – 2002) to obtain the electric field-dependent transmitted light intensity and the threshold voltage. An ac pulsed electric field (burst parameters: electric field ON cycle = 100 ms and OFF cycle = 100 ms, sine wave, frequency = 10 kHz) is applied to the sample to measure the response times (τ_{ON} and τ_{OFF}). The transmitted light intensity collected by the photodiode is fed to a digital oscilloscope (*Agilent* – DSO4000X) to record the time

dependence. The τ_{ON} and τ_{OFF} are defined as the time taken for the transmitted light intensity to vary from 10% to 90% and 90% to 10% of the maximum transmitted light intensity, respectively.
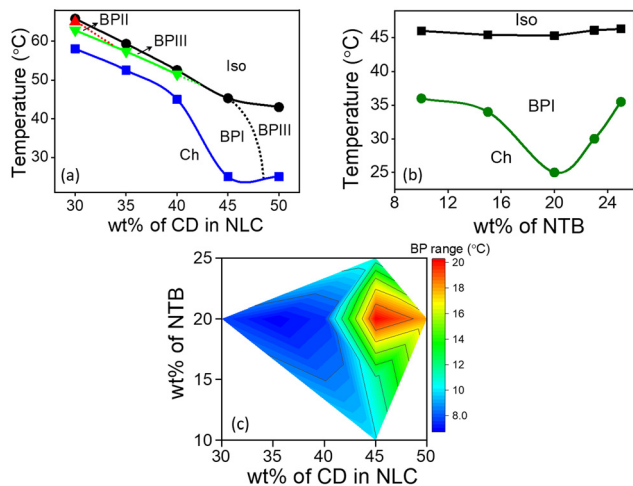
3. Results and discussion

3.1. Optimizing the host BPLC

The host BPLC comprising NTB, CD and NLC is prepared by optimizing the concentration of each of the constituents such that the BP exhibits maximum thermal range. The chemical structures, phase transition temperatures, and composition of different BPLC mixtures are provided in Fig. S1, Section S1, ESI.† Typically, LC compounds with a rigid bent-core are used to enhance the thermal range of BP.[44] In the present system, NTB, a liquid crystalline dimer with a flexible alkyl linker, which shows the twist-bend nematic phase, is strategically employed (as discussed later in this section) to increase the thermal stability of BP. The temperature-concentration phase diagrams obtained by varying the concentration of CD/NTB in NLC are shown in Fig. 1. The phases and the phase transition temperatures are determined using a polarizing optical microscope (POM) in conjunction with a temperature-controlled hot stage (for details, see 'Experimental section').

In the first set of experiments, the concentration of CD in NLC is varied from 30 to 50 wt%, with the concentration of NTB kept constant at 20 wt%. The partial temperature-concentration phase diagram thus obtained is shown in Fig. 1a. On cooling from the Iso phase, the composites with CD concentration ranging from 30 to 40 wt% exhibit BPIII, characterized by a dark foggy texture. The overall thermal range of BPIII in the mixtures is between 1 and 3 °C. On cooling further, platelet textures corresponding to the BPII and/or BPI phases appear, which eventually transform into a texture with small focal conics, characteristic of the Ch phase, at lower temperatures. For the mixture with 45 wt% of CD, a direct transition from Iso to BPI is observed with no signature of BPIII. Interestingly, for this composite, the BPI-Ch transition precipitously drops to 25 °C, and thus BPI exists over a thermal range of 20.3 °C. On increasing the CD concentration to 50 wt%, BPI vanishes completely, and the BPIII re-emerges with a thermal range of 18 °C. However, the phase is unstable at ambient temperatures, with Ch appearing at 25 °C.

Next, the concentration of CD is kept constant at 45 wt%, and the NTB concentration is varied from 10 to 25 wt%, as shown in the phase diagram, Fig. 1b. It may be noted that varying the concentration of NTB hardly affects the phase sequence and the Iso-BPI transition temperature. However, the transition temperature corresponding to the BPI-Ch shows a eutectic point with the thermal range of BPI being maximum (~20 °C) for the 20 wt% NTB composite (see Fig. 1b and c), clearly indicating the critical role of NTB in the thermal stability of the BP.

To further understand the role of NTB in stabilizing the BP, control experiments are carried out on a BP mixture consisting of a bent-core material[45] BLC, replacing NTB. The chemical structure and phase transition temperatures of BLC are presented in Fig. S1, ESI.† The mixture, with 20 wt% BLC and 45 wt% CD in NLC, exhibits a similar phase sequence with BPI

9688 | *J. Mater. Chem. C*, 2023, **11**, 9686–9694

This journal is © The Royal Society of Chemistry 2023

Fig. 1 Partial temperature-concentration phase diagrams of BPLC mixtures. The temperature *vs.* concentration (in weight%) of (a) CD in NLC (with NTB fixed at 20 wt%) and (b) NTB in (45 wt% CD in NLC) showing the thermal range of cubic and amorphous BPs. (c) The contour plot depicting the variation of the overall BP thermal range with respect to concentration of CD and NTB. The scale blue to red indicates the increasing thermal range of BP.

appearing on cooling from the Iso phase. However, the thermal range of BPI is found to be only ~3.5 °C, nearly six times lower compared to when NTB is added. The POM textures and the phase sequence are given in Fig. S4, Section S3 of ESI.† Thus, the liquid crystal dimeric (also known as bimesogenic) compound NTB, which exhibits the twist-bend nematic phase, is more effective in enhancing the thermal range of BP compared to BLC.

3.2. Effect of NTB on the thermal stability of BP

The thermal stabilization of BP largely depends on the elastic constants of the LC medium, as per Meiboom's theory.[46] The modified[47] free energy (F) expression of the blue phase per unit length of the disclination lines is given by

$$F = F_{core} + F_{interface} + F_2 + F_1 + \gamma F_{DTC} \qquad (1)$$

where F_2 is the integral over the surface surrounding the disclination line, F_1 is the Frank elastic energy in a region surrounding the disclination ($s = -1/2$), and F_{DTC} is the elastic energy of the DTC per unit length. $\gamma (= \sqrt{3}/2)$ is the ratio of the length of the DTC to that of the disclination line. The expressions for each of the terms are given below.

$$F_2 = -1/2\pi (K_{22} + K_{24}) \qquad (2)$$

where K_{24} is the saddle splay elastic constant

$$F_1 = 1/4\pi (K_{11} + K_{22} + K_{33}) \ln (R_{max}/r_c) \qquad (3)$$

where K_{11}, K_{22} and K_{33} are the splay, twist, and bend elastic constants, respectively. r_c is the radius of the core, and R_{max} is its cutoff radius.

$$F_{DTC} = 0.65 K_{22} + 0.23 K_{33} \qquad (4)$$

The terms F_{core} (= $a\Delta T\pi r_c^2$, where ΔT is the temperature distance to the Iso-BP transition) and $F_{interface}$ (= $2\pi r_c \sigma$, where σ

is the interfacial tension) are the excess free energy of the disclination core and the interfacial energy between the disclination core and bulk liquid crystal, respectively.

Among the five terms in eqn (1), F_{core} and $F_{interface}$ are independent of the elastic constants, and therefore only F_1, F_2 and F_{DTC} are considered for further discussions.

As already discussed, the BP is formed by a lattice of DTCs interspersed with a lattice of topological defects (disclination lines). Hence, for the BP to be stable with respect to the single helical Ch phase, the total energy should be minimized such that the energy cost of the disclinations is overcome by the stabilizing effect of DTC.[6–8,46,47] Additionally, the saddle splay elastic constant (K_{24}) is known to play a significant role in minimizing the free energy.[47–49]

With this background, the enhanced thermal stability of BP due to the addition of NTB can be understood as follows: the inclusion of BLC is known to reduce K_{33} owing to the bent-shaped molecules.[44] However, NTB with the chemical structure (see Fig. S1, ESI†) of a central flexible alkyl chain connecting the two phenyl groups is more conducive to bend deformations compared to BLC and hence exhibits ultra-low bend elastic constant.[48,49] Thus, the free energy component F_1 is minimized to a greater extent with the addition of NTB than when BLC is added (eqn (3)). Furthermore, the twist-bend nematic phase exhibited by NTB is known to undergo saddle-splay deformation.[48–50] Therefore, a finite value of the associated elastic constant, K_{24}, gives a negative contribution and reduces the free energy component, F_2 (according to eqn (2)). The term 0.23 K_{33} in F_{DTC} (eqn (4)) contributes to the further minimization of the free energy.

Thus the presence of NTB results in an overall reduction of the free energy leading to a thermally stable BP. It may be mentioned here that Coles *et al.* have achieved high thermal stability of BP in bimesogenic compounds[51] with chemical structures similar to that of NTB. Thus materials exhibiting twist-bend nematic phase may have an edge over conventional BLC materials to achieve enhanced thermal stability of BP. A similar trend has also been observed in our earlier reported works.[52,53]

3.3. The QD-BPLC system: stabilization of BPIII

As discussed above, the BPLC mixture with 45 wt% CD and 20 wt% NTB (denoted as BP45 hereafter) exhibits the highest thermal range of BPI, and is selected as the BPLC host for further studies with QDs. The POM textures and the corresponding selective reflection spectra obtained for the BP45 on cooling from Iso at 0.2 °C min⁻¹ are shown in Fig. S5, Section S3, ESI.† The BPI characterized by violet platelets appears just below the Iso phase, and on cooling further, the platelets turn bluish-green; eventually, Ch appears at 25 °C.

A small concentration of 0.005 wt% of QDs is added to BP45 to obtain the composite referred to as QD-BPLC hereafter. Details regarding the characterization of the QDs are given in the 'Experimental section' and Section S2, ESI† (Fig. S2 and S3).

On cooling the QD-BPLC from the Iso at 0.2 °C min⁻¹, a dark foggy texture is seen under the POM at 45 °C, and the texture remains intact until 11 °C. On cooling further, the Ch phase

This journal is © The Royal Society of Chemistry 2023

J. Mater. Chem. C, 2023, **11**, 9686–9694 | **9689**

appears with the characteristic tiny focal conic texture. The POM textures obtained for the composite in the Iso, BPIII and Ch phases are shown in Fig. S6, Section S4, ESI.† The bright spots seen in the textural images (Fig. 2a and Fig. S6, ESI†) are due to the aggregates of the QDs that are uniformly dispersed in the BP medium. As the size of the aggregates is only a few microns, the scattering from them is not visible to the naked eye, as will be evident from the actual images of the device shown in the later section.

It must be mentioned here that as both Iso and BPIII phases are optically isotropic, it is non-trivial to differentiate between the two phases using POM textural studies, especially in the presence of the scattering particles. Careful POM studies done using a POL quality microscope objective lens (×10) show faint foggy background in the BPIII and a dark field of view in Iso, as shown in Fig. 2a.

On application of an in-plane ac electric field (sine, 10 kHz), the dark foggy texture transforms to a bright birefringent texture. The appearance of the birefringent state corresponds to the unwinding of the helical structure (DTCs), a direct confirmation that the phase is indeed BPIII.[21–26] The POM textures obtained in the dark and field-induced birefringent states are shown in Fig. 3 and Fig. S11 (Section S9, ESI†). Thus, the phase sequence of the QD-BPLC is: Iso 45 °C BPIII 11 °C Ch, and the thermal range of BPIII is 34 °C (see Fig. 2b). The thermal range covers ambient, above- and sub-ambient temperatures. Thus the addition of a small concentration of QDs leads to the induction of BPIII with BPI completely disappearing from the phase sequence.

Determination of optical activity is a method to confirm the presence of a chiral phase, in this case, BPIII. This is done by rotating the analyzer from the crossed position (optic axes of the polarizer and analyzer being 90° with respect to each other) clockwise and anti-clockwise +/− 10°. A slight difference in brightness between the +10° and −10° positions (see Fig. S7, Section S5, ESI†), in conjunction with the optical isotropy, confirms that the mesophase is chiral. The presence of a chiral mesophase is further confirmed by circular dichroism studies. The spectra obtained for QD-BPLC show a clear signal indicating
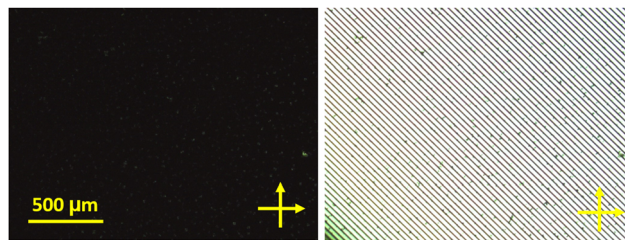

Fig. 3 The POM images of the QD-BPLC in the OFF state (left) and ON state (right) of BPIII. Temperature is kept constant at 25 °C.

optical activity in the BPIII and no peak in the Iso, on cooling the sample from Iso (see Fig. S8, Section S6, ESI†).

Further differential scanning calorimetry (DSC) experiments are carried out to determine the Iso-BPIII and BPIII-Ch phase transitions more accurately for QD-BPLC. The DSC thermograms obtained on the heating and cooling cycles (at the rate of 5 °C min^{-1}) are shown in Fig. S9, Section S7, ESI.† On heating, the Ch phase transforms to BPIII at 15.2 °C, and on heating further, Iso appears at 46.2 °C. On cooling, the phase transition temperatures corresponding to Iso-BPIII and BPIII-Ch occur at 45.1 °C and 14.1 °C, respectively. Thus, the BPIII thermal range obtained from DSC is ∼31 °C, both on heating and cooling, and is 3 °C less compared to what is obtained from the POM studies. The difference in thermal range is attributed to the effect of sample thickness; the DSC experiments are performed on a bulk sample, i.e., 20 mg in a 40 µl DSC cup, whereas POM studies are done on a thin film (∼8 µm thickness) sample. It is known from the literature[54] that the BP thermal range strongly depends on the sample thickness, thinner samples showing higher thermal range compared to thicker ones, explaining the disparity in the thermal range of BPIII obtained from the POM and DSC.

The addition of surface-functionalized nanoparticles such as QDs is known to stabilize BP and, more importantly, extend the thermal range of BPIII at the cost of cubic BP.[31,32] The QDs with sizes up to 10 nm can effectively get confined inside the core of disclination lines (∼10 nm in diameter), stabilizing the organization of the topological defects.[31–33] Moreover, the surface functionalised QDs, when doped in the BP system, are expected
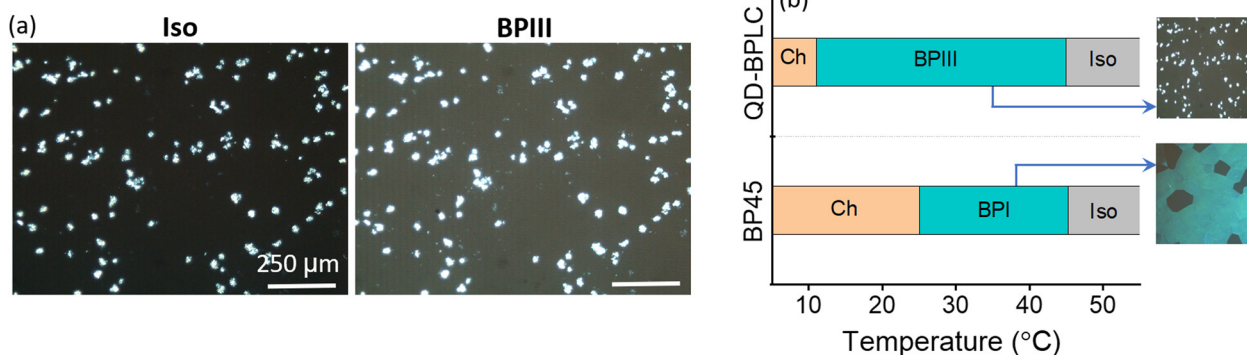

Fig. 2 (a) The POM images of QD-BPLC (kept between crossed polarizers, ×10 POL quality objective) captured while cooling the sample from Iso show the foggy background in BPIII and the dark field of view in Iso against bright scattering QDs. (b) The phase sequence of the BP45 and QD-BPLC mixtures depicting the blue phase thermal range enhancement and transformation of BPI to BPIII in the presence of QDs.

9690 | J. Mater. Chem. C, 2023, 11, 9686–9694

This journal is © The Royal Society of Chemistry 2023

to distribute non-uniformly within the disclination lines, stabilizing the amorphous BP over the more ordered BPI or BPII.[31] Additionally, the long chain ligands, *i.e.*, the ODA molecules tethered to the QDs, tend to interact with the LC molecules near the disclination lines reducing the free energy of the defect cores leading to close packing of the DTCs and hence lattice contraction.[55,56] This in turn results in increased chirality and thus induction/stabilization of BPIII.

Thus, this study clearly brings out the significant role of NTB, a material with ultra-low bend elastic constant[48,49] (as discussed in Section 3.2) and that of QDs, the zero-dimensional nanomaterial, in the thermal stabilization of BPs.

The POM studies are also carried out on BPLC mixtures by varying the concentration of QDs in BP45 from as low as 0.001 wt% to 0.1 wt% to understand the QD concentration dependence on the thermal range of BPIII. The BPIII starts appearing for the mixture with 0.002 wt%, although the range is only 4 °C. When the concentration of QDs is > 0.005 wt%, the BPIII still exists over a large thermal range, but the scattering from the particles increases (see Fig. S10, Section S8, ESI†), which in turn affects the optical properties (transmittance) of BPIII. Thus, the maximum thermal range of BPIII with minimal scattering from the particles is obtained for 0.005 wt%.

It must also be mentioned here that the addition of QDs enhances the BPIII thermal range only if the CD concentration is sufficiently high in the host BPLC. In the case of lower CD concentration composites, *e.g.*, 30, 35 and 40 wt%, the addition of QDs has no effect on the overall thermal range of BPIII (see Table S1, ESI†). Also, the temperature-dependent absorption and emission spectroscopy carried out on the QD-BPLC composite show that the emission intensity is insignificant as the concentration of QD in the host BPLC is quite low.

3.4. Electro-optical studies

The QD-BPLC is filled in an ITO-coated in-plane LC test cell to carry out the electro-optical switching studies. The procedure used is described in the 'Experimental section'. All the experiments are carried out at an ambient temperature of 25 °C, unless otherwise stated.

3.4.1. Electric-field induced optical transmittance. Fig. 3 shows the POM images of the achromatic dark (no electric field: OFF) and bright birefringent (electric field-induced: ON) states of the BPIII in the QD-BPLC. The images are captured at 25 °C by keeping the polarizer and analyzer in crossed positions. The electric field (25 V μm^{-1}, sine, 10 kHz) applied in the plane of the substrates unwinds the DTC structure of BPIII with LC molecules orienting along the field direction resulting in a birefringent state. The pattern seen in the bright state is due to the inter-digitated electrodes of the in-plane cell magnified five times by the microscope objective. The switching between bright and dark states is highly reversible over several cycles of application and removal of the electric field.

The transmitted light intensity through the sample (normalized with respect to the intensity values obtained in parallel and crossed-polarizer conditions without the sample in the optical path) as a function of the applied electric field, in both increasing and decreasing cycles, is shown in Fig. 4. The intensity, which is close to 0% in the pristine state, increases with the increasing electric field and saturates at a value of ∼80% for electric fields 20 V μm^{-1} and above.

3.4.2. Threshold electric field. From the electric field dependence of transmitted light intensity (Fig. 4), the threshold field for switching between dark and bright states is calculated to be 3.5 V μm^{-1}. The value is lower than what is obtained for the polymer stabilized BPIII systems[31] and is on par with the lowest values reported for low molecular weight systems (see Tables 1 and 2, Section 3.5). It may be mentioned here that the presence of QDs is known to enhance the dielectric anisotropy of LC systems, which in turn leads to a reduction in the threshold electric field of the QD-BPLC system.[57]

3.4.3. Hysteresis and contrast ratio. The electric field-dependent transmitted intensity values collected in the increasing field cycle nearly overlap with those obtained in the decreasing cycle leading to a hysteresis-free behaviour (see Fig. 4). The contrast ratio, defined as the ratio of maximum to minimum transmitted intensity, is calculated from the transmittance curve.[58] The value thus obtained is 3300:1, a high intrinsic contrast ratio without the need for additional compensation films or complicated device geometries.[59]

3.4.4. Response times. The experimental procedure used for the determination of response times, the switch ON (τ_{ON}) and switch OFF (τ_{OFF}), are given in the 'Experimental section' and Section S9 of the ESI.† Fig. 5a and b show the response time data collected as a function of the applied electric field at two fixed temperatures, 35 °C and 25 °C. While the τ_{OFF} is nearly invariant with the electric field, the τ_{ON} decreases monotonically with increasing electric field. For electric fields > 15 V μm^{-1}, both τ_{ON} and τ_{OFF} reach sub-millisecond values. For example, the τ_{ON} and τ_{OFF} are ∼0.2 ms and 0.3 ms, respectively, at 25 V μm^{-1}. The addition of nanoparticles is known to reduce ionic impurities in the LC medium,[57] and hence the ultra-fast sub-millisecond response time in the BPIII of the QD-BPLC system.
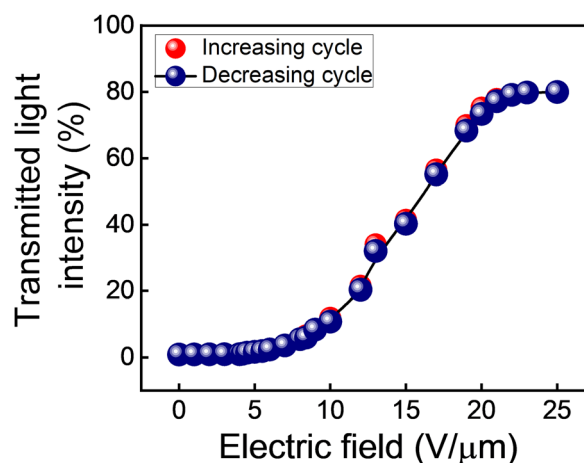

Fig. 4 Electric field dependence of transmitted light intensity in increasing and decreasing cycles for the QD-BPLC sample at 25 °C. The solid line drawn through the data points is a guide to the eye.

This journal is © The Royal Society of Chemistry 2023

J. Mater. Chem. C, 2023, **11**, 9686–9694 | **9691**

Table 1 Electro-optic parameters of QD-BPLC

| | | | | Response time | |
BPIII thermal range (°C)	Threshold electric field (V μm⁻¹)	Contrast ratio	Transmitted light intensity (%)	τ_{ON} (ms)	τ_{OFF} (ms)
34	3.5	3300 : 1	OFF state: 0.02% ON state: 80%	0.24 ± 0.005	0.29 ± 0.005

Table 2 Comparison of device parameters of QD-BPLC with those reported in the literature

| Thermal stability | | | Electro-optic parameters | | | | | | Transmitted light intensity (%) | | |
| | Transition temp. (°C) | | | | | | | | | | |
BPIII range (°C)	Iso – BPIII	BPIII – Ch	E_{th} (V μm⁻¹)	τ_{ON} (ms)	τ_{OFF} (ms)	E_{op} (V μm⁻¹)	Hysteresis (%)	OFF state	ON state	LC composites
10.8	32.5	21.7	3.1	1.16	0.96	10	—	0	22	Rod-like nematic + chiral dopant[42]
16	35	19	5	1.1	1.1	20	0.057	—	—	Rod-like nematic + chiral dopant[43]
20	40	20	—	—	—	—	—	—	—	Rod-like nematic + chiral dopant + bent core compound[35]
20	100	80	—	<10	<10	15	—	—	—	Bent core nematic + chiral dopant[36]
15	37	22	2	15	5	6	0	—	—	Bent core nematic + chiral dopant[37]
7.2	28.4	21.2	4	0.4	0.8	14	0	0	89	Rod-like nematic + chiral dopant + T-shaped[39]
8	36	28	3	1.6	3.9	13	—	0.9	85	T-shaped nematic + chiral dopant[40]
8	49	41	3	8	8	10	—	0.85	55	Chiral T-shaped compound (single component[38]
32.9	24.7	−8.2	—	200	600	12	—	0.7	80	Chiral T-shaped compound (single component)[41]
83	83	0	5	<0.1	0.07	18.5	0.49	—	—	Polymer stabilization of (Rod-like nematic + chiral dopant[30]
66.6	83.6	17	10	<0.1	<0.2	40	—	—	—	Polymer scaffold + rod-like nematic [31]
17.5	144.5	127	—	—	—	—	—	—	—	Chiral liquid crystal + QD[32]
7.2	146.2	139	—	—	—	—	—	—	—	Chiral liquid crystal + QD[33]
34	45	11	3.5	0.24	0.29	25	0.03	0.02	80	Rod-like nematic + chiral dopant + twist-bend nematic compound + QD (*Present work*)

E_{th}: threshold electric field; E_{op}: operating electric field; —: data not available.

The response times are also measured as a function of temperature at a fixed electric field of 25 V μm⁻¹, as shown in Fig. 5c. The τ_{ON} remains almost invariant with the temperature except at 20 °C, while τ_{OFF} increases upon cooling. The response time of BPIII is directly proportional to the rotational viscosity

according to the relationship[38]

$$\tau = \frac{\gamma_R P^2}{k(2\pi)^2} \qquad (5)$$

where γ_R is the rotational viscosity, 'P' is the helical pitch, and 'k' is the average elastic constant. Typically, the rotational viscosity of LCs increases upon cooling due to increased molecular ordering. Hence the τ_{OFF}, which is purely driven by the collective motion of the LC molecules in the absence of an electric field, increases upon cooling. However, even at 20 °C, the response times are relatively fast, *i.e.*, τ_{ON} and τ_{OFF} are ∼0.5 and 1 ms, respectively.

3.5. BPIII device

A prototype display device incorporating QD-BPLC with an active area of 1 cm × 1.2 cm is fabricated to demonstrate the electro-optical switching at ambient temperatures. A pair of polarizers (P, A) are fixed on either side of the LC test cell filled with the sample and the polarization axes are kept 90° (crossed polarizers) with respect to each other. The device is illuminated with a white light from an LED lamp. An ac electric field (sine, 10 kHz) is applied to the sample using a function generator/amplifier setup (see 'Experimental section' for more details). Fig. 6 (top row) shows the images of the device captured at room temperature using a digital camera. The achromatic dark state switches to a bright state on application of an electric field
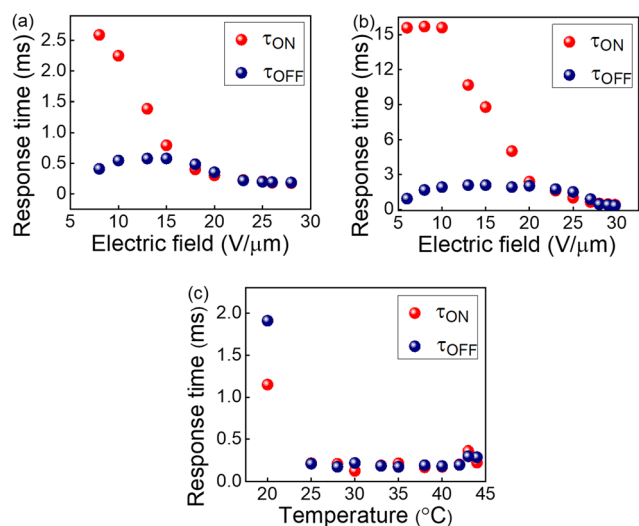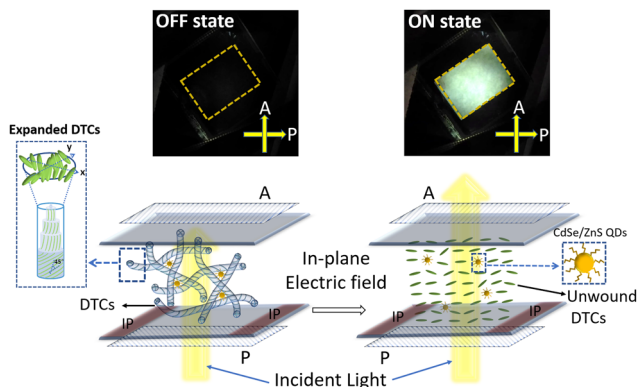

Fig. 5 Electric field dependence of response times in BPIII of the QD-BPLC at (a) 35 °C and (b) 25 °C. (c) Thermal dependence of response times at a fixed electric field of 25 V μm⁻¹.

Fig. 6 (top) Digital images of the BPIII device at room temperature (25 °C) in the OFF and ON states. The electric field applied is 25 V μm⁻¹. The dashed square encompasses the active area of 1 cm×1.2 cm. (bottom) Schematic representation of the electro-optic switching: (left) the random arrangement of DTCs in the pristine OFF state and (right) unwinding of DTCs on the application of the electric field. P, A and IP denote polarizer, analyser and in-plane electrodes, respectively.

(25 V μm⁻¹), demonstrating an excellent contrast between the two states. A video of the electro-optical switching is shown in Movie S1, ESI.† As already discussed, the aggregates of the QDs do not scatter light in the OFF state when viewed with the naked eye (see Fig. 6) and are visible only at a high magnification (10× and above) under POM (see Fig. 2a and Fig. S6, ESI†).

The electro-optic parameters of the device, *viz.*, threshold electric field, response time, optical transmittance, and contrast ratio, are summarized in Table 1. The values obtained are also compared with those reported in the literature (see Table 2). It may be seen from the table that the thermal stability and response times of BPIII exhibited by QD-BPLC are better than that of the low molecular weight systems and are comparable to that of the polymer-stabilized systems reported in the literature. Furthermore, the BPIII also exhibits hysteresis-free performance. The display device fabricated using the composite has been highly stable under ambient conditions for more than a year. The switching behaviour of BPIII in the QD-BPLC system is schematically represented in Fig. 6.

Thus, QD-BPLC, a low molecular weight liquid crystal composite prepared by the strategic addition of NTB and QDs, exhibits a wide thermal range of BPIII spanning above ambient, ambient and sub-ambient temperatures. Furthermore, the composite exhibits an operating electric field comparable to the values reported in the literature (see Table 2). The system also exhibits sub-millisecond response time, hysteresis-free transmittance and high contrast ratio and therefore has the potential to be used as an active material for high-performance LC display devices.

4. Conclusion

A BPIII with enhanced thermal stability and sub-millisecond electro-optical response is achieved in a low molecular weight LC system by the strategic addition of NTB, a twist-bend nematic dimer and surface-functionalized QDs. The ultra-low bend elastic constant and the saddle-splay deformations of NTB combined with the size-compatible QDs getting confined inside the defect cores reduce the free energy of the system, stabilizing the topological defects and hence the BPIII over a wide temperature range of 34 °C covering above-ambient, ambient and sub-ambient. Notably, the addition of QDs transforms the cubic BPI to amorphous BPIII. The optimized QD-BPLC device shows excellent electro-optic performance on the application of an ac electric field: an achromatic dark state that switches to a bright state with a sub-millisecond response time (~0.2 ms) and excellent contrast ratio (~3300 : 1). The device also exhibits robust, hysteresis-free switching and is found to be thermally and electrically stable for more than two years. Thus, the QD-BPLC system is highly promising to be used in display devices, with the potential to perform on par with the latest OLED technology.

Author contributions

The manuscript was written through the contributions of all authors. All authors have given approval to the final version of the manuscript. NK: conceptualization and planning of experiments, data collection and analysis, and writing the first draft and editing the manuscript. VS: data analysis and editing the manuscript. KFC: synthesis of BLC. GGN: validation of experiments, overall supervision, project administration, funding acquisition, and editing & reviewing of the manuscript.

Conflicts of interest

There are no conflicts to declare.

Acknowledgements

Notes and references

1 D.-K. Yang and S.-T. Wu, *Fundamentals of liquid crystal devices*, John Wiley & Sons, 2014.
2 W. Den Boer, *Active matrix liquid crystal displays: fundamentals and applications*, Elsevier, 2011.
3 T. Uchida, *Jpn. J. Appl. Phys.*, 2014, **53**, 03CA02.
4 K.-H. Kim and J.-K. Song, *NPG Asia Mater.*, 2009, **1**, 29–36.
5 H.-W. Chen, J.-H. Lee, B.-Y. Lin, S. Chen and S.-T. Wu, *Light Sci. Appl.*, 2018, **7**, 17168.
6 P. P. Crooker, *Liq. Cryst.*, 1989, **5**, 751–775.
7 T.-H. Lin, C.-W. Chen and Q. Li, *Anisotropic nanomaterials*, Springer, 2015, pp. 337–378.

This journal is © The Royal Society of Chemistry 2023

J. Mater. Chem. C, 2023, **11**, 9686–9694 | **9693**

8 H. F. Gleeson, R. Miller, L. Tian, V. Görtz and J. Goodby, *Liq. Cryst.*, 2015, **42**, 760–771.

9 E. Dubois-Violette and B. Pansu, *Mol. Cryst. Liqu. Cryst.*, 1988, **165**, 151–182.

10 M. A. Rahman, S. M. Said and S. Balamurugan, *Sci. Technol. Adv. Mat.*, 2015, **16**(3), 033501.

11 L. Wang and Q. Li, *Adv. Funct. Mat.*, 2016, **26**, 10–28.

12 J. Yang, J. X. Zhang, X. Zhang, L. Wang, W. Feng and Q. Li, *Adv. Mater.*, 2021, **33**(14), 2004754.

13 Y. Yang, L. Wang, H. Yang and Q. Li, *Small Sci.*, 2021, **1**(6), 2100007.

14 L. Wang, A. M. Urbas and Q. Li, *Adv. Mater.*, 2020, **32**(41), 1801335.

15 Q. Gong and X. Hu, *Photonic crystals: principles and applications*, Pan Stanford, 2019.

16 J. Yan, Z. Luo, S.-T. Wu, J.-W. Shiu, Y.-C. Lai, K.-L. Cheng, S.-H. Liu, P.-J. Hsieh and Y.-C. Tsai, *App. Phys. Lett.*, 2013, **102**, 011113.

17 X. Xu, Z. Liu, Y. Liu, X. Zhang, Z. Zheng, D. Luo and X. Sun, *Adv. Opt. Mater.*, 2018, **6**, 1700891.

18 V. Sridurai, M. Mathews, C. V. Yelamaggad and G. G. Nair, *ACS Appl. Mater. Interfaces*, 2017, **9**, 39569–39575.

19 H. Coles and S. Morris, *Nat. Photon.*, 2010, **4**, 676–685.

20 Y. Yang, X. Zhang, Y. Chen, X. Yang, J. Ma, J. Wang, L. Wang and W. Feng, *ACS Appl. Mater. Interfaces*, 2021, **13**(34), 41102–41111.

21 H. Stegemeyer, T. Blümel, K. Hiltrop, H. Onusseit and F. Porsch, *Liq. Cryst.*, 1986, **1**, 3–28.

22 H.-S. Kitzerow, P. Crooker and G. Heppke, *Phys. Rev. Lett.*, 1991, **67**, 2151.

23 L. Rao, Z. Ge, S. Gauza, K.-M. Chen and S.-T. Wu, *Mol. Cryst. Liq. Cryst.*, 2010, **527**, 30/[186]–142/[198].

24 K.-M. Chen, S. Gauza, H. Xianyu and S.-T. Wu, *J. Disp. Technol.*, 2010, **6**, 49–51.

25 Z. Ge, S. Gauza, M. Jiao, H. Xianyu and S.-T. Wu, *Appl. Phys. Lett.*, 2009, **94**, 101104.

26 Y. Chen, J. Yan, J. Sun, S.-T. Wu, X. Liang, S.-H. Liu, P.-J. Hsieh, K.-L. Cheng and J.-W. Shiu, *Appl. Phys. Lett.*, 2011, **99**, 201105.

27 H. Lee, H. J. Park, O. J. Kwon, S. J. Yun, J. H. Park, S. Hong and S. T. Shin, *SID Symposium Digest of Technical Papers*, 2011, **42**, 121–124.

28 H.-S. Kitzerow, *Emerging liquid crystal technologies IV*, 2009, **7232**, 723205.

29 H. Kikuchi, M. Yokota, Y. Hisakado, H. Yang and T. Kajiyama, *Nat. Mat.*, 2002, **1**, 64–68.

30 M. S. Kim and L.-C. Chien, *Soft Matter*, 2015, **11**, 8013–8018.

31 S. S. Gandhi, M. S. Kim, J. Y. Hwang and L. C. Chien, *Adv. Mat.*, 2016, **28**, 8998–9005.

32 E. Karatairi, B. Rožič, Z. Kutnjak, V. Tzitzios, G. Nounesis, G. Cordoyiannis, J. Thoen, C. Glorieux and S. Kralj, *Phys. Rev. E: Stat., Nonlinear, Soft Matter Phys.*, 2010, **81**, 041703.

33 G. Cordoyiannis, M. Lavrič, M. Trček, V. Tzitzios, I. Lelidis, G. Nounesis, M. Daniel and Z. Kutnjak, *Front. Phys.*, 2020, 315.

34 R. K. Khan and P. Ramarao, *J. Appl. Phys.*, 2021, **129**, 024702.

35 K. V. Le, S. Aya, Y. Sasaki, H. Choi, F. Araoka, K. Ema, J. Mieczkowski, A. Jakli, K. Ishikawa and H. Takezoe, *J. Mater. Chem.*, 2011, **21**, 2855–2857.

36 S. Taushanoff, K. Van Le, J. Williams, R. J. Twieg, B. Sadashiva, H. Takezoe and A. Jákli, *J. Mat. Chem.*, 2010, **20**, 5893–5898.

37 R. K. Khan, G. Mohiuddin, N. Begum, S. Turlapati, R. V. Nandiraju, B. K. Debbarma and S. Ghosh, *ACS Appl. Mater. Interfaces*, 2022, **14**, 42628–42634.

38 M. Sato and A. Yoshizawa, *Adv. Mat.*, 2007, **19**, 4145–4148.

39 A. Yoshizawa, M. Kamiyama and T. Hirose, *Appl. Phys. Express*, 2011, **4**, 101701.

40 H. Iwamochi and A. Yoshizawa, *Appl. Phys. Express*, 2008, **1**, 111801.

41 H. Iwamochi, T. Hirose, Y. Kogawa and A. Yoshizawa, *Chem. Lett.*, 2010, **39**, 170–171.

42 H.-Y. Chen, S.-F. Lu and Y.-C. Hsieh, *Opt. Express*, 2013, **21**, 9774–9779.

43 H.-Y. Chen, S.-F. Lu, P.-H. Wu and C.-S. Wang, *Liq. Cryst.*, 2017, **44**, 473–478.

44 S.-T. Hur, M.-J. Gim, H.-J. Yoo, S.-W. Choi and H. Takezoe, *Soft Matter*, 2011, **7**, 8800–8803.

45 K. Fodor-Csorba, A. Jákli and G. Galli, *Macromol. Symp.*, 2004, **218**, 81–88.

46 S. Meiboom, J. P. Sethna, P. Anderson and W. Brinkman, *Phys. Rev. Lett.*, 1981, **46**, 1216.

47 J.-i Fukuda, *Phys. Rev. E: Stat., Nonlinear, Soft Matter Phys.*, 2012, **85**, 020701.

48 V. Borshch, Y.-K. Kim, J. Xiang, M. Gao, A. Jákli, V. P. Panov, J. K. Vij, C. T. Imrie, M.-G. Tamba and G. H. Mehl, *Nat. Commun.*, 2013, **4**, 1–8.

49 V. Panov, J. Song, G. Mehl and J. Vij, *Crystals*, 2021, **11**(6), 621.

50 J. V. Selinger, *Liq. Cryst. Rev.*, 2018, **6**, 129–142.

51 H. J. Coles and M. N. Pivnenko, *Nature*, 2005, **436**, 997–1000.

52 N. Khatun, V. Sridurai, R. K. Gupta, S. Nath, M. B. Kanakala, S. Garain, A. S. Achalkumar, C. V. Yelamaggad and G. G. Nair, *J. Phys. Chem. B*, 2021, **125**, 11582–11590.

53 N. Khatun, V. Sridurai, R. Pujar, M. B. Kanakala, S. K. Choudhary, G. U. Kulkarni, C. V. Yelamaggad and G. G. Nair, *J. Mol. Liq.*, 2021, **325**, 115059.

54 S.-K. Hong, G.-H. Lim and H. Kikuchi, *Mol. Cryst. Liq. Cryst.*, 2009, **511**, 248/[1718]–1254/[1724].

55 M. Ravnik, G. P. Alexander, J. M. Yeomans and S. Žumer, *Proc. Natl. Acad. Sci. U. S. A.*, 2011, **108**(13), 5188–5192.

56 K. Orzechowski, M. Tupikowska, O. Strzeżysz, T. M. Feng, W. Y. Chen, L. Y. Wu, C. T. Wang, E. Otón, M. M. Wójcik, M. Bagiński, P. Lesiak, W. Lewandowski and T. R. Woliński, *ACS Nano*, 2022, **16**(12), 20577–20588.

57 S. Singh, *Crystals*, 2019, **9**, 475.

58 J. Chen, W. Cranton and M. Fihn, *Handbook of visual display technology*, Springer, 2016.

59 S. Khosla, S. Lal and A. Devi, *AIP Conf. Proc.*, 2021, **2352**, 020037.